Journal of Power Sources 195 (2010) 7691–7700

Contents lists available at ScienceDirect

Journal of Power Sources

journal homepage: www.elsevier.com/locate/jpowsour

New molten salt systems for high-temperature molten salt batteries: LiF–LiCl–LiBr-based quaternary systems

Syozo Fujiwara [a,*], Minoru Inaba [b], Akimasa Tasaka [b]

[a] Technology Development Center, Energy Company, Panasonic Corporation Matsushita-cho, Moriguchi, Osaka 570-8511, Japan
[b] Department of Molecular Chemistry and Biochemistry, Faculty of Science and Engineering, Doshisha University, Kyotanabe, Kyoto 610-0321, Japan

ARTICLE INFO

Article history:
Received 25 October 2009
Received in revised form 18 May 2010
Accepted 19 May 2010
Available online 25 May 2010

Keywords:
Molten salt
Thermal battery
Electrolyte
Simulation
Ionic conductivity
Melting point

ABSTRACT

To develop novel multi-component molten salt systems more effectively, we developed a simulative technique using the CALPHAD (Calculation of Phase Diagram and Thermodynamics) method to estimate the ionic conductivity and the melting point. The validity of this new simulative technique was confirmed by comparing the simulated ionic conductivities and melting points of typical high-temperature molten salts, such as LiF–LiCl–LiBr, LiF–LiBr–KBr, LiCl–LiBr–KBr, and LiCl–LiBr–LiI, with those reported data in the literature or experimentally obtained.

This simulative technique was used to develop new quaternary molten salt systems for use as electrolytes in high-temperature molten salt batteries (called thermal batteries). The targets of the ionic conductivity and the melting point were set at 2.0 S cm^{-1} and higher at 500 °C, and in the range of 350–430 °C, respectively, to replace the LiCl–KCl system (1.85 S cm^{-1} at 500 °C) within the conventional design of the heat generation system for thermal batteries. Using the simulative method, six kinds of novel quaternary systems, LiF–LiCl–LiBr–MX (M = Na and K; X = F, Cl, and Br), which contain neither environmentally instable anions such as iodides nor expensive cations such as Rb^+ and Cs^+, were proposed. Experimental results showed that the LiF–LiCl–LiBr–0.10NaX (X = Cl and Br) and LiF–LiCl–LiBr–0.10KX (X = F, Cl, and Br) systems meet our targets of both the ionic conductivity and the melting point.

1. Introduction

High-temperature molten salt batteries, which generally consist of a high-temperature molten salt electrolyte (such as LiCl–KCl), a Li–Al alloy anode, and a FeS_2 cathode, have been developed for electric vehicle applications [1,2]. This combination has also been adopted into so-called thermally activated batteries or thermal batteries [3], because of their high output power, superior stability in long-term storage, and so on. The thermal batteries can produce enormous high power drain due to the high ionic conductivity of the molten salt electrolyte. To obtain the high power, they should be operated within a proper temperature range between the melting point of the salt at ca. 400 °C and the decomposition temperature of the positive electrode material (ca. 600 °C for FeS_2 [4]). Once after activated, they work until reaching either the capacity limit of active materials or the solidification temperature of the molten salt electrolyte [5].

Though the thermal batteries have a high discharge rate-capability, further improvement of the output power is required in many applications. The conventional LiCl–KCl molten salt system has a melting point of 350 °C and an ionic conductivity of 1.85 S cm^{-1} at 500 °C. To further improve the discharge rate-capability of the thermal batteries, the molten salt electrolyte should have a higher ionic conductivity and an appropriate melting point to be fitted to a conventional heat generation system developed for the LiCl–KCl system. We set the target of the ionic conductivity at 2.0 S cm^{-1} or higher at 500 °C to further increase the output power of the high-temperature molten salt batteries, and the target for the melting point within a temperature range of 350–430 °C to replace the conventional LiCl–KCl electrolyte with newly developed electrolyte systems.

Several new multi-component salt systems containing bromides and iodides have been investigated to improve the ionic conductivity and to reduce the melting point [6,7]. Iodide-containing salt systems have a high conductivity and a sufficiently low melting point, and hence seem to be suitable for controlling the balance between the conductivity and the melting point [8–11]. In our previous study [5,12], it was shown that LiF–LiCl–LiBr–LiI, LiF–LiCl–LiI, and LiF–LiBr–LiI systems have higher ionic conductivities (~3 S cm^{-1} at 500 °C) than the conventional LiCl–KCl system and have low melting points (below 400 °C). However, they showed instability at high temperatures in dried air, decomposing at temperatures higher than 280 °C owing to the oxidation of

* Corresponding author. Tel.: +81 6 6991 4639; fax: +81 6 6998 3179.
E-mail address: fujiwara.syozou@jp.panasonic.com (S. Fujiwara).

0378-7753/$ – see front matter © 2010 Elsevier B.V. All rights reserved.
doi:10.1016/j.jpowsour.2010.05.032

Table 1
Comparison of simulated and reported data in the literature for eutectic composition, melting point, and ionic conductivity of conventional molten salt systems.

Molten salt system	Simulated data in the present study			Reported data in the literature		
	Composition (mol%)	Melting point (°C)	Ionic conductivity (S cm^{-1} at 1000 °C)	Composition (mol%)	Melting point (°C)	Ionic conductivity (S cm^{-1} at 1000 °C)
LiF–LiCl–LiBr	21–23–56	440	6.94	21–23–56	443	6.52
LiF–LiBr–KBr	3–60–37	325	4.55	3–63–34	312	4.47
LiCl–LiBr–KBr	25–37–38	330	4.39	25–37–38	322	4.19
LiCl–LiBr–LiI	24–19–57	370	5.89	24.3–19–56.7	368	6.13

iodides by oxygen, and hence they are excluded in the present study.

In the present study, we first developed a simulative technique to design the ionic conductivity and the melting point to develop new multi-component molten salt systems more effectively. Using this technique, we proposed brand-new quaternary molten salt systems based on the LiF–LiCl–LiBr ternary system (LiF–LiCl–LiBr–MX (M = Na and K; X = F, Cl, and Br)), which contain neither environmentally instable anions such as iodides nor expensive cations such as Rb^+ and Cs^+. We also evaluated their ionic conductivities and melting points experimentally, and discussed the validity of this new simulative technique and the effect of the fourth mono salt to the LiF–LiCl–LiBr system on the ionic conductivity and the melting point.

2. Experimental

2.1. Materials

LiF, LiBr, NaF, NaCl, KF, KCl and KBr from Kanto Kagaku, and LiCl and NaBr from Kojundo Chemical Laboratory were used as raw materials. All these materials were of reagent grade with purity higher than 99.9%. After these salts were dried separately at 200 °C under vacuum for 48 h, they were mixed to obtain four kinds of ternary molten salt systems, LiF–LiCl–LiBr, LiF–LiBr–KBr, LiCl–LiBr–KBr, and LiCl–LiBr–LiI listed in Table 1, and six kinds of quaternary systems, LiF–LiCl–LiBr–MX (M = Na and K; X = F, Cl, and Br) listed in Tables 3–8, respectively, at their eutectic compositions.

2.2. Ionic conductivity and melting point measurements

The ionic conductivity of the molten salts was measured by the alternating current (AC) impedance method reported by Yuzuru Sato et al. [13]. Prior to measurements, the cell constant K was determined with a molten salt with a well-accepted ionic conductivity, LiCl–KCl (1.85 S cm^{-1} at 500 °C) [14]. The ionic conductivity κ was obtained from the resistance R of the sample using the following equation:

$$\kappa = K \times R^{-1} \quad (1)$$

The preparation of the molten salts and conductivity measurements were conducted in a glove box filled with dried air. The dew point in the glove box was maintained below −45 °C.

The melting points of the molten salts were determined by differential thermal analysis (DTA) using a TG-DTA system (Bruker Axs, TG-DTA2000SA).

2.3. Simulative technique

Phase diagrams and eutectic compositions of molten salt systems of different compositions and temperatures were calculated from thermodynamic data using a FactSage software (GTT Technologies GmbH), which is based on the CALPHAD (Calculation of Phase Diagram and Thermodynamics) method [15].

The ionic conductivity of a mixed molten salt system was obtained from the equivalent conductivities and the molar ratio of constituent salts at the eutectic composition obtained from the phase diagram of the system using the CALPHAD method. For example, in the case of a ternary salt system consisting of salt 1, 2, and 3, we calculated the apparent equivalent conductivity, the apparent gram equivalent, the apparent density, and the ionic conductivity at a given temperature as follows:

(1) Apparent equivalent conductivity γ_{mix}:

$$\gamma^t_{mix} = X_1 * \gamma^t_1 + X_2 * \gamma^t_2 + X_3 * \gamma^t_3 \quad (2)$$

(2) Apparent gram equivalent eq_{mix}:

$$eq_{mix} = X_1 * eq_1 + X_2 * eq_2 + X_3 * eq_3 \quad (3)$$

(3) Apparent density ρ^t_{mix}:

$$\rho^t_{mix} = X_1 * r\rho^t_1 + X_2 * \rho^t_2 + X_3 * \rho^t_3 \quad (4)$$

(4) Ionic conductivity κ_{mix}:

$$\kappa^t_{mix} = \frac{\gamma^t_{mix}}{eq^*_{mix}\rho^t_{mix}} \quad (5)$$

Here X_1, X_2, and X_3 denote the mole fractions, γ^t_1, γ^t_2, and γ^t_3 equivalent conductivities, eq_1, eq_2, and eq_3 denote the gram equivalents, ρ^t_1, ρ^t_2, and ρ^t_3 denote the densities of salts 1, 2, and 3, respectively, at a temperature t (K).

The melting point and the molar fraction of each mixed melt were obtained from the eutectic composition of the phase diagrams determined with the CALPHAD method, and the equivalent conductivity and the density of each salt were obtained from the literature [16].

3. Results and discussion

3.1. Conventional molten salt systems

To validate our simulation method, we calculated the ionic conductivities and the melting points for typical ternary systems, LiF–LiCl–LiBr, LiF–LiBr–KBr, LiCl–LiBr–KBr, and LiCl–LiBr–LiI, which have been developed for use in thermal batteries [5–10]. The phase diagrams obtained using the CALPHAD method are plotted in Figs. 1–4, and the simulated ionic conductivities and melting points are compared with those reported in the literature [5–10] in Table 1. Here the ionic conductivities were compared using the values at 1000 °C, because each mono salt has a high melting point, *e.g.* LiF (m.p. 842 °C). The calculated ionic conductivity and melting point of each system well agreed to those reported in the literature, which confirmed that our calculation technique with the CALPAHD method is a powerful tool to predict important properties of molten salt electrolytes, that is, the ionic conductivity and the melting point.

We also checked the validity of our experimental techniques for the ionic conductivity and the melting point measurements.

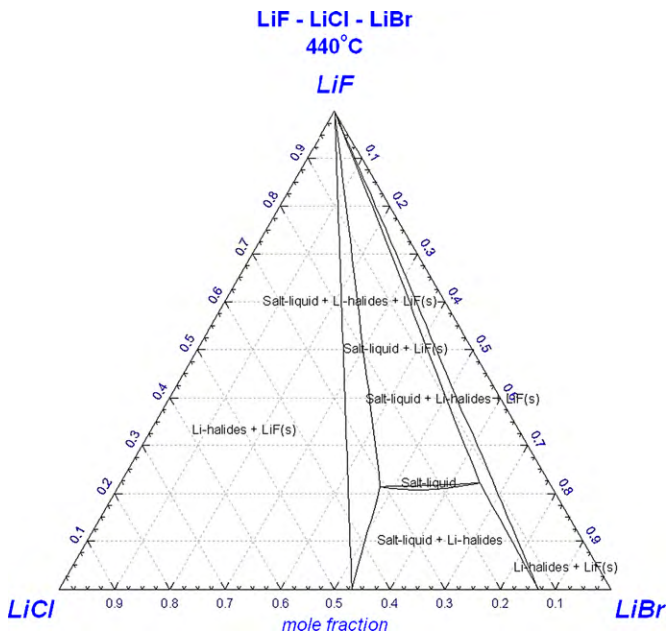

Fig. 1. Phase diagram of LiF–LiCl–LiBr at 440 °C.

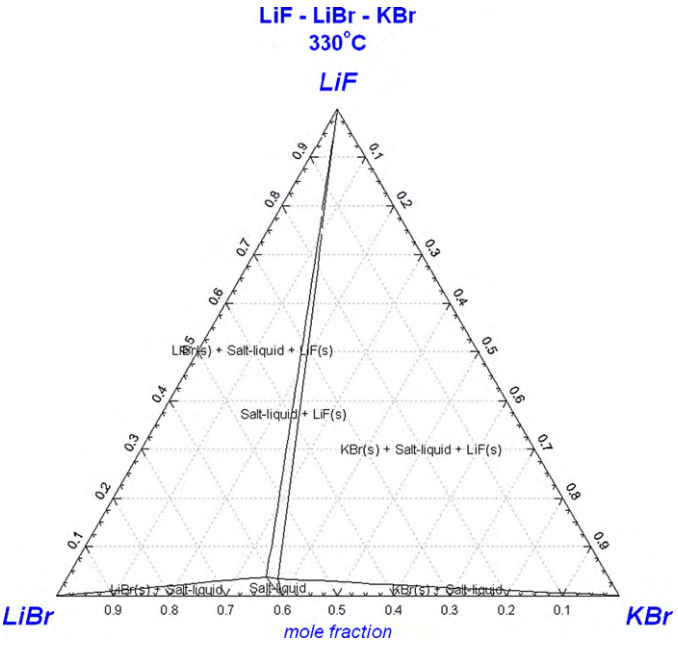

Fig. 2. Phase diagram of LiF–LiBr–KBr at 330 °C.

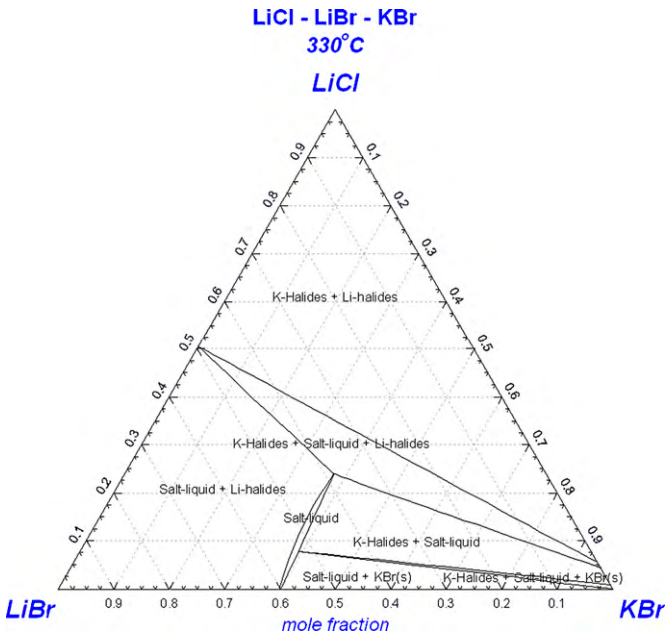

Fig. 3. Phase diagram of LiCl–LiBr–KBr at 330 °C.

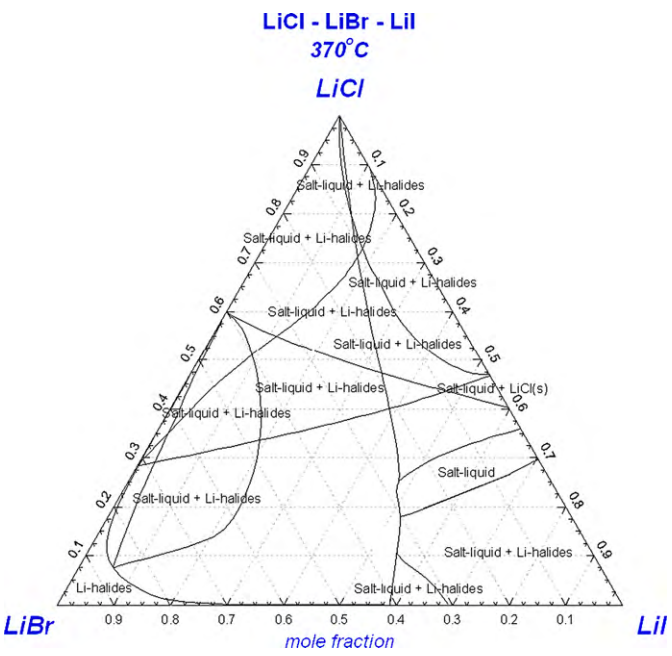

Fig. 4. Phase diagram of LiCl–LiBr–LiI at 370 °C.

The ionic conductivities and the melting points obtained experimentally in the present study and reported in the literature for LiF–LiCl–LiBr, LiF–LiBr–KBr, LiCl–LiBr–KBr, and LiCl–LiBr–LiI are summarized in Table 2. Here the ionic conductivities were compared at 500 °C, considering the conventional design of thermally activated batteries. The ionic conductivities and the melting points measured experimentally in the present study well agreed to those reported in the literature [5–10], which confirmed that they were measured properly by our experimental techniques.

Table 2
Comparison of melting points and ionic conductivities reported in the literature and obtained experimentally in the present study for conventional molten salt systems.

Molten salt system	In the literature		Experimental Data in the present study	
	Melting point (°C)	Ionic conductivity (S cm^{-1} at 500 °C)	Melting point (°C)	Ionic conductivity (S cm^{-1} at 500 °C)
LiF–LiCl–LiBr	443	3.39	440	3.41
LiF–LiBr–KBr	312	1.66	320	1.69
LiCl–LiBr–KBr	310	1.64	320	1.72
LiCl–KCl	354	1.83	350	1.85

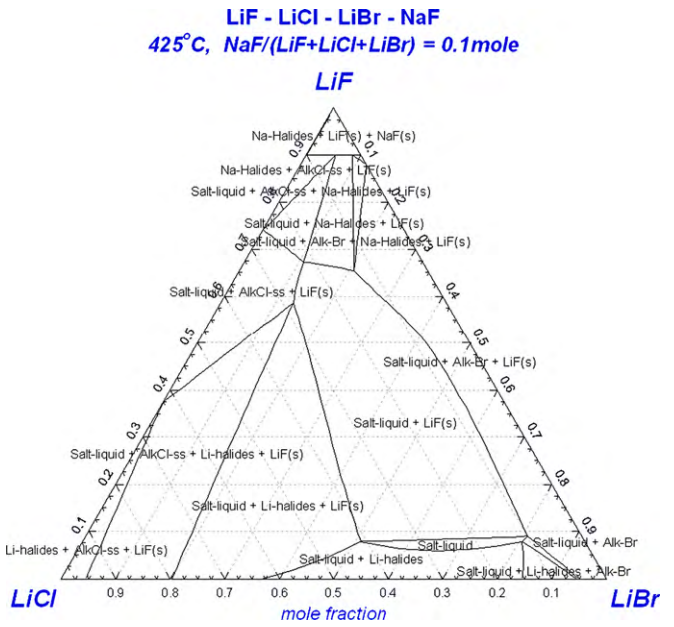

Fig. 5. Phase diagram of LiF–LiCl–LiBr–0.10NaF at 425 °C.

3.2. New quaternary molten salt systems

Of the conventional molten salt systems in Table 2, only the LiF–LiCl–LiBr system had an ionic conductivity value (3.41 S cm^{-1} at 500 °C) that satisfied our target of the ionic conductivity (>2 S cm^{-1} at 500 °C). However, its melting point (440 °C) was a little higher than our target (350–430 °C). We examined the effect of the fourth-salt addition to the LiF–LiCl–LiBr system on the ionic conductivity and the melting point, which has not been reported yet. We chose NaF, NaCl, NaBr, KF, KCl, and KBr, as fourth salts from alkaline halides. Here we excluded alkaline halides containing environmentally instable anions such as iodides and expensive cations as Cs^+ and Rb^+.

First we fixed the molar ratio of the forth salt at $x = 0.01$, 0.03, 0.10, 0.20 or 0.30, and calculated an eutectic composition for each quaternary system (LiF–LiCl–LiBr–xMX (M = Na and K; X = F, Cl, and Br). Typical phase diagrams for $x = 0.1$, that is, LiF–LiCl–LiBr–0.10NaF, LiF–LiCl–LiBr–0.10KF, LiF–LiCl–LiBr–0.10NaCl, LiF–LiCl–LiBr–0.10KCl, LiF–LiCl–LiBr–0.10NaBr, and LiF–LiCl–LiBr–0.1KBr, obtained using the CALPAHD method are shown in Figs. 5–10, respectively. At each eutectic composition, the ionic conductivity and the melting point were calculated using the method described in the previous section. The ionic conductivity at 500 °C and the melting point of each salt system were also obtained experimentally at its eutectic composition, and were compared with those obtained by simulation.

3.2.1. LiF–LiCl–LiBr–xNaF and LiF–LiCl–LiBr–xKF systems

Simulated data for the eutectic compositions, the ionic conductivity (at 1000 °C), and the melting point of the LiF–LiCl–LiBr–xNaF and LiF–LiCl–LiBr–xKF ($x = 0.01$, 0.03, 0.10, 0.20 or 0.30) systems are listed in Tables 3 and 4, respectively, as well as the ionic conductivity (at 500 °C) and the melting point obtained experimentally. The simulative data revealed that the melting point decreases with increasing the content of NaF and KF up to $x = 0.10$ and then increased for both systems. The melting point at $x = 0.10$ (425 °C) was lower than that of the ternary LiF–LiCl–LiBr system (430 °C), but higher at other values of x. This tendency can be correlated with the change in the F^- content in the total anions. From the viewpoint of elemental composition, the melting point of the quaternary sys-

Table 3
Comparison of simulated and experimentally obtained data for melting point and ionic conductivity for new LiF–LiCl–LiBr–xNaF ($x = 0.01$, 0.03, 0.10, and 0.30) systems developed in the present study.

Molten salt system	Simulated data							Experimental data	
	Eutectic composition (mol%)	Li content (mol%)	Na content (mol%)	F content (mol%)	Cl content (mol%)	Br content (mol%)	Melting point (°C)	Ionic conductivity (S cm^{-1} at 1000 °C)	Melting point (°C)	Ionic conductivity (S cm^{-1} at 500 °C)
LiF–LiCl–LiBr–NaF	20–22–57–1	99.0	1.0	20.8	21.6	57.6	440	6.86	440	3.33
LiF–LiCl–LiBr–NaF	16–22–59–3	97.0	3.0	19.4	22.2	58.4	440	6.86	435	3.30
LiF–LiCl–LiBr–NaF	6–22–62–10	90.0	10.0	16.6	21.8	61.6	425	6.72	440	3.11
LiF–LiCl–LiBr–NaF	1–35–44–20	80.0	20.0	20.5	35.6	43.9	475	6.63	–	–
LiF–LiCl–LiBr–NaF	1–13–56–30	70.0	30.0	31.4	12.5	56.1	565	6.41	–	–

Table 4
Comparison of simulated and experimentally obtained data for melting point and ionic conductivity for new LiF–LiCl–LiBr–*x*KF (*x* = 0.01, 0.03, 0.10, and 0.30) systems developed in the present study.

Molten salt system	Simulated data							Experimental data	
	Eutectic composition (mol%)	Li content (mol%)	K content (mol%)	F content (mol%)	Cl content (mol%)	Br content (mol%)	Melting point (°C)	Ionic conductivity ($S cm^{-1}$ at 1000 °C)	Melting point (°C)	Ionic conductivity ($S cm^{-1}$ at 500 °C)
LiF–LiCl–LiBr–KF	19–22–58–1	99.0	1.0	20.4	22.0	57.6	440	6.89	440	3.36
LiF–LiCl–LiBr–KF	16–21–60–3	97.0	3.0	19.1	21.2	59.7	435	6.81	435	3.28
LiF–LiCl–LiBr–KF	6–21–63–10	90.0	10.0	15.6	21.0	63.4	420	6.57	420	2.68
LiF–LiCl–LiBr–KF	1–39–40–20	80.0	20.0	20.3	39.5	40.2	500	6.34	–	–
LiF–LiCl–LiBr–KF	2–14–54–30	70.0	30.0	31.7	14.0	54.3	610	6.03	–	–

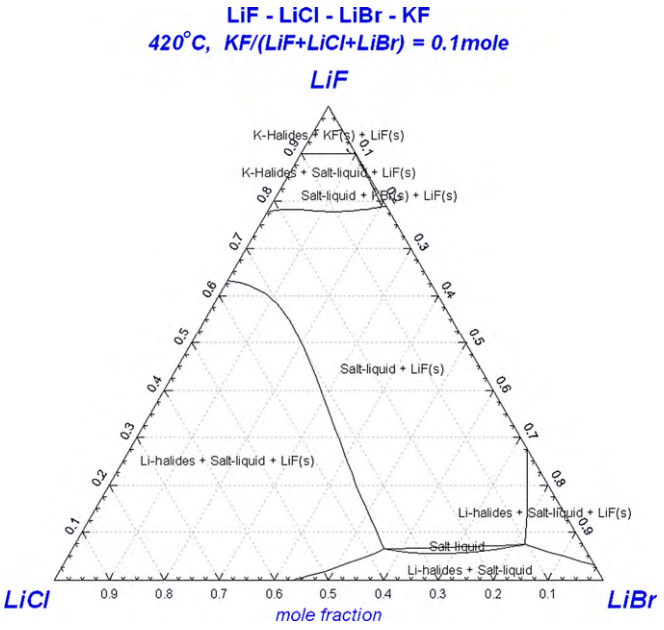

Fig. 6. Phase diagram of LiF–LiCl–LiBr–0.10KF at 420 °C.

tems increased with increasing the F^- content in the total anion content at each eutectic composition.

The observed effect of the F^- content on the melting point is probably brought about by the small ionic radius of F^- anions. Fluoride anions have the smallest anion size among the anions used in the present study; hence, the effect of F^- anions on the reduction of the total stability of the crystal structure in the solid state is the weakest. Therefore the melting point increased with an increase in the F^- concentration in the total anions. In addition to the size effect of F^- anion, we also found the size effect of cations, which will be discussed in the following sections.

We experimentally confirmed the variation of the melting point predicted by simulation for both systems. The lowest melting point (420 °C) was obtained at $x = 0.1$ as predicted for the LiF–LiCl–LiBr–*x*KF system, where the ionic conductivity satisfied

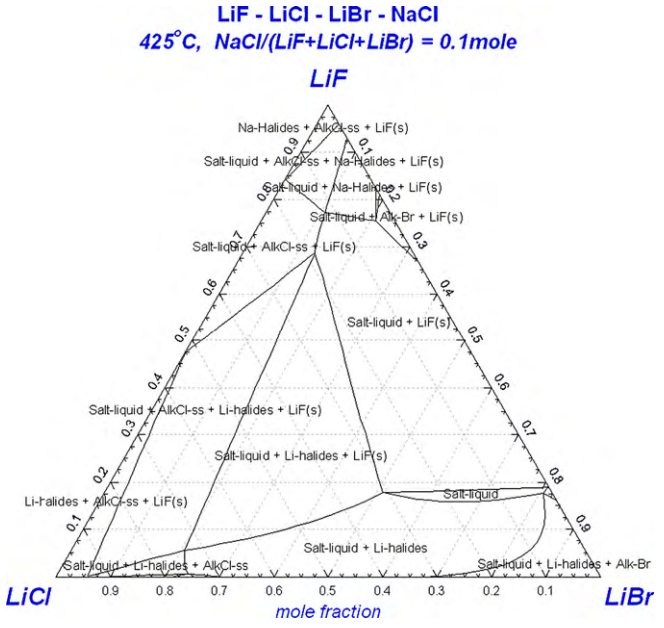

Fig. 7. Phase diagram of LiF–LiCl–LiBr–0.10NaCl at 425 °C.

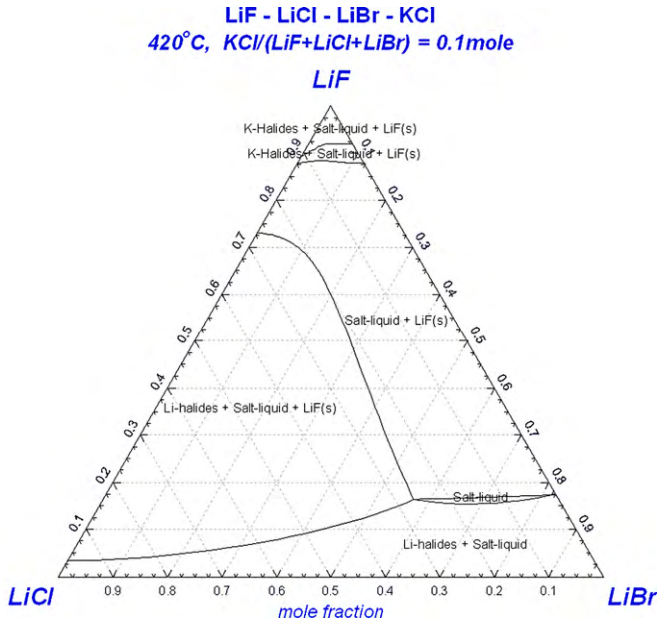

Fig. 8. Phase diagram of LiF–LiCl–LiBr–0.10KCl at 420 °C.

our target (>2.0 S cm^{-1} at 500 °C). For the LiF–LiCl–LiBr–*x*NaF system, the lowest melting point (435 °C) was obtained at a slightly lower content of $x = 0.03$, which was higher than our target of the melting point (350–430 °C).

3.2.2. *LiF–LiCl–LiBr–xNaCl and LiF–LiCl–LiBr–xKCl systems*

Simulated and experimentally measured data for LiF–LiCl–LiBr–*x*NaCl and LiF–LiCl–LiBr–*x*KCl ($x = 0.01, 0.03, 0.10, 0.20$ or 0.30) systems are listed in Tables 5 and 6, respectively. The simulated data suggested that the melting point and the ionic conductivity decreased monotonously with increasing the molar ratio of NaCl or KCl for each system. One of the major reasons for the decrease in the melting point by the addition of NaCl or KCl is due to a reduced concentration of F^- anions at the eutectic composition in each system as shown in Tables 5 and 6, which is in agreement with the

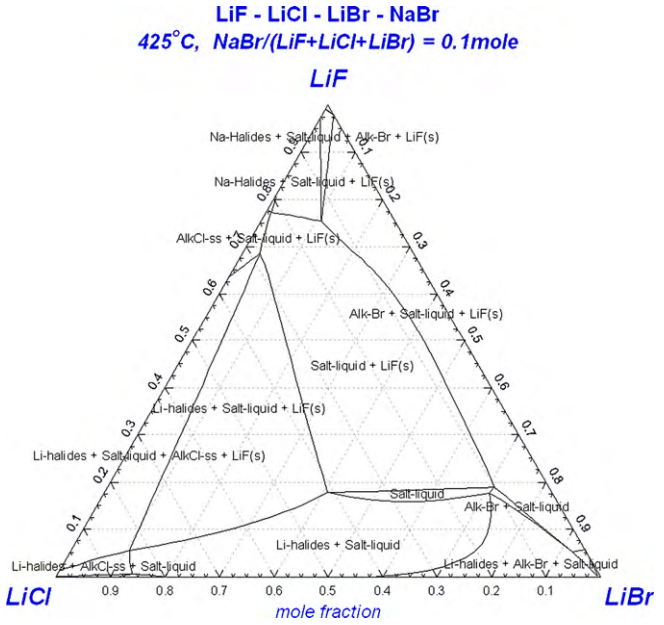

Fig. 9. Phase diagram of LiF–LiCl–LiBr–0.10NaBr at 425 °C.

Table 5
Comparison of simulated and experimentally obtained data for melting point and ionic conductivity for new LiF–LiCl–LiBr–*x*NaCl ($x = 0.01$, 0.03, 0.10, and 0.30) systems developed in the present study.

Molten salt system	Simulated data								Experimental data	
	Eutectic composition (mol%)	Li content (mol%)	Na content (mol%)	F content (mol%)	Cl content (mol%)	Br content (mol%)	Melting point (°C)	Ionic conductivity (S cm^{-1} at 1000 °C)	Melting point (°C)	Ionic conductivity (S cm^{-1} at 500 °C)
LiF–LiCl–LiBr–NaCl	21–21–57–1	99.0	1.0	20.5	22.0	57.5	440	6.90	445	3.50
LiF–LiCl–LiBr–NaCl	19–20–58–3	97.0	3.0	19.2	23.0	57.8	435	6.83	445	3.44
LiF–LiCl–LiBr–NaCl	15–13–62–10	90.0	10.0	15.6	22.6	61.8	425	6.59	430	3.16
LiF–LiCl–LiBr–NaCl	11–10–59–20	80.0	20.0	11.2	30.3	58.5	410	6.29	–	–
LiF–LiCl–LiBr–NaCl	9–15–46–30	70.0	30.0	8.4	45.3	46.3	405	6.02	460	3.15

Table 6
Comparison of simulated and experimentally obtained data for melting point and ionic conductivity for new LiF–LiCl–LiBr–*x*KCl (*x* = 0.01, 0.03, 0.10, and 0.30) systems developed in the present study.

Molten salt system	Simulated data							Experimental data	
	Eutectic composition (mol%)	Li content (mol%)	K content (mol%)	F content (mol%)	Cl content (mol%)	Br content (mol%)	Melting point (°C)	Melting point (°C)	Ionic conductivity ($S cm^{-1}$ at 500 °C)
LiF–LiCl–LiBr–KCl	20–21–58–1	99.0	1.0	20.4	21.5	58.1	440	435	3.32
LiF–LiCl–LiBr–KCl	19–20–58–3	97.0	3.0	19.0	22.5	58.5	435	433	3.23
LiF–LiCl–LiBr–KCl	15–12–63–10	90.0	10.0	14.6	22.4	63.0	420	415	2.77
LiF–LiCl–LiBr–KCl	10–8–62–20	80.0	20.0	9.5	28.4	62.1	405	–	–
LiF–LiCl–LiBr–KCl	6–7–57–30	70.0	30.0	6.1	36.9	57.0	385	–	–

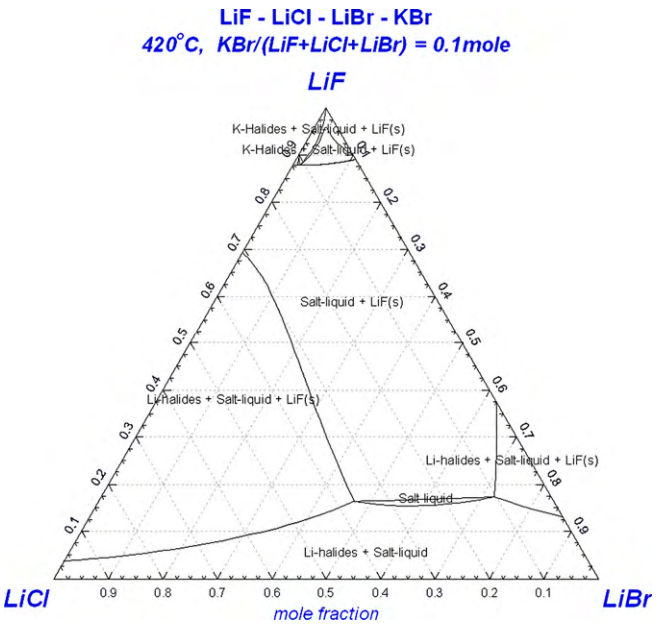

Fig. 10. Phase diagram of LiF–LiCl–LiBr–0.10KBr at 420 °C.

discussion in the previous section. In contrast, the ionic conductivity was decreased by the addition of NaCl or KCl, because of a reduced concentration of Li^+ cations at the eutectic composition. This is because the equivalent conductivity of Li^+ cations is higher than that of Na^+ or K^+ cations.

In the case of LiF–LiCl–LiBr–*x*NaCl, the experimentally obtained melting points and the tendency for the ionic conductivity well agreed with the respective simulative data at low NaCl contents of $x \leq 0.1$, and the melting point and the ionic conductivity at $x = 0.10$ satisfied our targets. On the other hand, the melting point at $x = 0.30$ were rather higher than that expected from the simulated data. We observed that the crystallization process of the LiF–LiCl–LiBr–0.30NaCl melt was much faster than that of LiF–LiCl–LiBr–*x*NaCl with lower NaCl contents. Though we have not completely clarified the reason at present, there may be an effect of inhomogeneity during the crystallization process, owing to a kinetically fast crystallization of some unknown phase containing Na^+ cations.

In the case of LiF–LiCl–LiBr–*x*KCl, the experimentally obtained melting points and the tendency of the ionic conductivity well agreed to that of the simulated data up to $x = 0.10$, though the ionic conductivity at $x = 0.10$ ($2.77\ S\ cm^{-1}$) seems to be slightly lower than that expected from the simulated trend in the ionic conductivity. In addition to the effect of Na^+ cations, we also found the size effect of K^+ cation, which will be discussed in the following sections. The melting point and the ionic conductivity of the LiF–LiCl–LiBr–0.10KCl system satisfied our targets.

3.2.3. *LiF–LiCl–LiBr–xNaBr and LiF–LiCl–LiBr–xKBr systems*

Simulated and experimentally measured data for LiF–LiCl–LiBr–*x*NaBr and LiF–LiCl–LiBr–*x*KBr ($x = 0.01$, 0.03, 0.10, 0.20 or 0.30) systems are listed in Tables 7 and 8, respectively. For both systems, the tendencies of the melting point and the ionic conductivity were similar to those for LiF–LiCl–LiBr–*x*NaCl and LiF–LiCl–LiBr–*x*KCl systems, and the melting point and the ionic conductivity decreased monotonously with increasing the content of NaBr or KBr. These effects are again attributed to a decrease in F^- anion concentration, as was observed for LiF–LiCl–LiBr–*x*NaCl and LiF–LiCl–LiBr–*x*KCl systems in the previous section.

Table 7
Comparison of simulated and experimentally obtained data for melting point and ionic conductivity for new LiF–LiCl–LiBr–NaBr (x = 0.01, 0.03, 0.10, and 0.30) systems developed in the present study.

Molten salt system	Simulated data								Experimental data	
	Eutectic composition (mol%)	Li content (mol%)	Na content (mol%)	F content (mol%)	Cl content (mol%)	Br content (mol%)	Melting point (°C)	Ionic conductivity (S cm^{-1} at 1000 °C)	Melting point (°C)	Ionic conductivity (S cm^{-1} at 500 °C)
LiF–LiCl–LiBr–NaBr	20–22–57–1	99.0	1.0	20.6	21.9	57.5	440	6.88	440	3.41
LiF–LiCl–LiBr–NaBr	19–22–56–3	97.0	3.0	19.2	22.1	58.7	435	6.78	435	3.41
LiF–LiCl–LiBr–NaBr	15–22–53–10	90.0	10.0	15.6	21.5	62.9	425	6.44	430	3.17
LiF–LiCl–LiBr–NaBr	11–28–41–20	80.0	20.0	11.2	27.9	60.9	410	6.01	–	–
LiF–LiCl–LiBr–NaBr	9–36–25–30	70.0	30.0	8.5	36.1	55.4	405	5.61	465	3.07

Table 8
Comparison of simulated and experimentally obtained data for melting point and ionic conductivity for new LiF–LiCl–LiBr–xKBr (x = 0.01, 0.03, 0.10, and 0.30) systems developed in the present study.

Molten salt system	Simulated data								Experimental data	
	Eutectic composition (mol%)	Li content (mol%)	K content (mol%)	F content (mol%)	Cl content (mol%)	Br content (mol%)	Melting point (°C)	Ionic conductivity (S cm^{-1} at 1000 °C)	Melting point (°C)	Ionic conductivity (S cm^{-1} at 500 °C)
LiF–LiCl–LiBr–KBr	20–22–57–1	99.0	1.0	20.4	22.0	57.6	440	6.84	435	3.35
LiF–LiCl–LiBr–KBr	19–21–57–3	97.0	3.0	18.8	21.4	59.8	435	6.66	430	3.18
LiF–LiCl–LiBr–KBr	15–21–54–10	90.0	10.0	14.6	21.2	64.1	420	6.09	415	2.73
LiF–LiCl–LiBr–KBr	10–20–50–20	80.0	20.0	9.8	19.7	70.5	400	5.41	–	–
LiF–LiCl–LiBr–KBr	6–18–46–30	70.0	30.0	6.4	18.0	75.6	380	4.82	–	–

The experimental results confirmed that the addition of NaBr or KBr as a fourth mono salt to the LiF–LiCl–LiBr system was effective for lowering the melting point, though the ionic conductivity decreased slightly. For LiF–LiCl–LiBr–*x*NaBr and LiF–LiCl–LiBr–*x*KBr system, the melting point and the ionic conductivity at $x = 0.10$, and at $x = 0.03$ and 0.10 satisfied our targets, respectively. The experimentally obtained melting points and the tendency of the ionic conductivity of the LiF–LiCl–LiBr–*x*NaBr and LiF–LiCl–LiBr–*x*KBr systems were very similar to that of the LiF–LiCl–LiBr–*x*NaCl and LiF–LiCl–LiBr–*x*KCl systems, respectively, in the previous section. The ionic radii of Cl^- (1.81 Å) and Br^- (1.96 Å) are similar to each other, when compared with other anions, F^- (1.33 Å) and I^- (2.2 Å). Hence the effects of NaCl and NaBr addition as the fourth salt on the total stability of the crystal structure in the solid state and on the cation–anion interactions in the liquid state would be similar, and these effects resulted in similar tendency in the melting point and the ionic conductivity.

Though we have so far discussed mainly the effects of anions on the melting point and the ionic conductivity, we observed clear size effects of cations. For example, the addition of potassium halides decreased both the melting point and the ionic conductivity more significantly than the addition of sodium halides at a given content. One reason for these effects is probably brought about by the ionic radius of K^+ (1.38 Å) cation larger than that of Li^+ (0.76 Å) or Na^+ (1.02 Å) cation. The large K^+ cation reduces the total stability of the crystal structure in the solid states more significantly than Li^+ or Na^+ cation, and this effect resulted in slightly lowering the melting points. On the other hand, the addition of K^+ cation affects the ionic conductivity more than the addition of Na^+ cation, because of its larger ionic size than that of Li^+ or Na^+ cation. Furthermore the smaller electronegativity of K^+ cation (0.81) than that of Li^+ (0.98) or Na^+ (0.93) cation may decrease the ionic character and increase the covalent character between anion and cation. Therefore the addition of larger K^+ cation resulted in lower ionic conductivities of the new molten salt systems and these effects became more remarkable as the concentration of K^+ cation increased.

These effects, cation–anion interactions, were not considered in our simulation in the present study. However, they were important for predicting the properties of molten salts more precisely, and are one of our major subjects to be discussed in the future.

3.3. Optimized compositions

In the present study, the final goal is to develop new quaternary molten salts systems that meet our targets of the ionic conductivity >2 S cm^{-1} at 500 °C and the melting point in the range of 350–430 °C. The best compromise between the melting point and the ionic conductivity for each quaternary LiF–LiCl–LiBr–*x*MX (M = Na and K; X = F, Cl, and Br) system in Tables 3–8 mostly lies at $x = 0.10$, except for NaF. (In the LiF–LiCl–LiBr–*x*NaF system, no composition satisfied our targets.) A closer look in Tables 3–8 revealed that for the three LiF–LiCl–LiBr–0.10NaX (X = F, Cl, and Br) systems containing Na^+, the elemental compositions are very similar (Li^+: 90, Na^+: 10, F^-: 15.6–16.6, Cl^-: 21.5–22.6, Br^-: 61.6–62.9 mol%), and the simulated melting points and the ionic conductivities were nearly equal to one another (425 °C and 6.44–6.72 S cm^{-1} at 1000 °C). In addition, the experimentally obtained melting points and the ionic conductivities for LiF–LiCl–LiBr–0.10NaCl and LiF–LiCl–LiBr–0.10NaBr were nearly equal to each other (430 °C and 3.16–3.17 S cm^{-1} at 500 °C). These are not strange coincidences, but the three LiF–LiCl–LiBr–0.10NaX (X = F, Cl, and Br) systems are essentially the same eutectic composition. Because the concentrations of F^-, Cl^-, and Br^- anions at the resulting eutectic composition being higher than 10%, the anion composition can be adjusted by changing the molar ratio of constituent salts of LiF, LiCl, and LiBr to become an eutectic composition as it should be, even if NaF, NaCl, or NaBr was added within a molar ratio of $x \leq 0.10$. This fact is also true for the LiF–LiCl–LiBr–0.01 and 0.03NaX (X = F, Cl, and Br) systems, and shows the validity of our simulation method using thermodynamic data. The strong resemblance among the phase diagrams of the three LiF–LiCl–LiBr–0.10NaX (X = F, Cl, and Br) systems at 425 °C shown in Figs. 5, 7 and 9 also supports that they have the same eutectic composition. Minor differences are observed in the three phase diagrams, but these are caused by the inaccuracy of the thermodynamic data of individual mono salts used for simulation. Though the eutectic composition is identical among the LiF–LiCl–LiBr–0.10NaX (X = F, Cl, and Br) systems, the experimentally obtained ionic conductivity and melting point of the LiF–LiCl–LiBr–0.10NaF system were slightly higher (440 °C) and lower (3.11 S cm^{-1} at 500 °C), respectively, than the other two systems, which we do not clarify the reason at present.

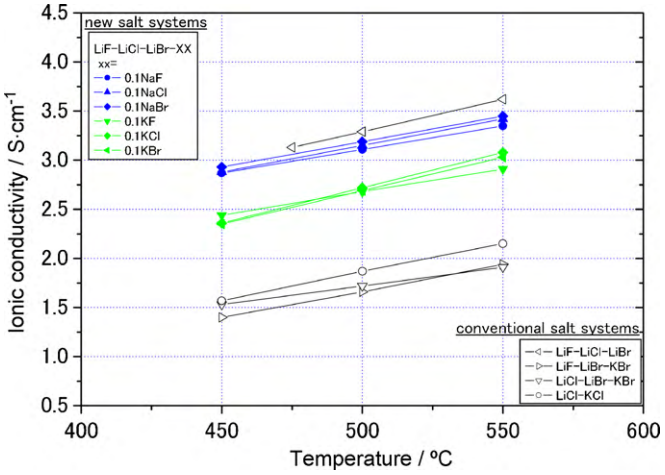

Fig. 11. Temperature dependencies of ionic conductivity of various molten salt systems.

The LiF–LiCl–LiBr–*x*KX (X = F, Cl, and Br) systems also have the same eutectic compositions at KX molar ratios $x \leq 0.10$. For example, the elemental compositions are also very similar (Li^+: 90, K^+: 10, F^-: 14.6–15.6, Cl^-: 21.2–22.4, Br^-: 63.0–63.3 mol%), and the simulated and experimentally obtained melting points and ionic conductivities were nearly equal to one another (simulated: 420 °C and 6.09–6.57 S cm^{-1} at 1000 °C; measured: 415–420 °C and 2.68–2.77 S cm^{-1} at 500 °C). Strong resemblance among the phase diagrams 420 °C was also observed for the three systems as shown in Figs. 6, 8 and 10.

The temperature dependence of the ionic conductivity for the six new quaternary molten salt systems, described as LiF–LiCl–LiBr–0.10MX (M = Na and K; X = F, Cl, and Br) in the range 450–550 °C are shown in Fig. 11, together with those for conventional salt systems (LiF–LiCl–LiBr, LiF–LiBr–KBr, LiCl–LiBr–KBr, and LiCl–KCl). In the case of the LiF–LiCl–LiBr system, the lower temperature limit was set at 475 °C to avoid solidification. The temperature dependencies of the new quaternary molten salt systems are almost the same as that of the conventional LiCl–KCl system. It is therefore expected that the discharge rate-capability can be improved by the use of new quaternary systems because of their high ionic conductivity, and a similar temperature dependence of discharge characteristics would be expected in practical battery applications.

4. Conclusions

To improve discharge rate-capability of high-temperature molten salt batteries, novel quaternary molten salt systems based on the LiF–LiCl–LiBr system were investigated without adding envi-

ronmentally instable anions such as iodides or expensive cations such as Cs, Rb, etc. To develop quaternary molten salt systems effectively, we established a simulative technique using the CALPHAD method to estimate the ionic conductivities and the melting points of multi-component molten salts systems.

We confirmed the validity of this new simulative technique, by comparing the simulated ionic conductivity and melting point data for typical high-temperature molten salts with reported values in the literature or experimentally obtained data.

Using the new simulative method, we proposed and evaluated brand-new type of quaternary molten salt systems based on the conventional ternary LiF–LiCl–LiBr system, such as LiF–LiCl–LiBr–NaF, LiF–LiCl–LiBr–NaCl, LiF–LiCl–LiBr–NaBr, LiF–LiCl–LiBr–KF, LiF–LiCl–LiBr–KCl, and LiF–LiCl–LiBr–KBr. The LiF–LiCl–LiBr–0.10NaX (X = Cl and Br) and LiF–LiCl–LiBr–0.10KX (X = F, Cl, and Br) systems experimentally meet our targets in both the ionic conductivity (>2.0 S cm^{-1} at 500 °C) and the melting point (350–430 °C) to be fitted within the conventional design of the heat generation system for thermally activated batteries.

It is therefore concluded that the new simulative technique with the CALPAHD method is a powerful tool to estimate the most important characteristics of molten salt electrolytes, such as the ionic conductivity and the melting point, and that the use of the newly developed molten salt systems as an electrolyte is expected to improve the discharge rate-capability of high-temperature molten salt batteries. Cell tests using these new molten salt systems are now in progress.

It is also important to understand the effect of interactions between cations and anions to predict the properties of multi-component molten salt systems more precisely in the future, considering more practical usage of the new simulative technique to develop new molten salt systems.

References

[1] T.D. Kaun, M.C. Hash, G.L. Henriksen, A.N. Jansen, D.R. Vissers, Materials and Mechanisms of High Temperature Lithium Sulfide Batteries, Conference: 2. Chilean Lithium Symposium, Santiago, Chile, 1994, pp. 171–192.
[2] T.D. Kaun, P.A. Nelson, L. Redey, D.R. Vissers, G.L. Henriksen, Electrochimica Acta 38 (9) (1993) 1269–1287.
[3] R.A. Guidotti, The 27th International Technical Conference of the Society for the Advancement of Material and Process Engineering (SAMPE): Diversity into the Next Century, Albuquerque, NM, 1995, pp. 807–818.
[4] A.G. Ritchie, P. Carter, The 38th Power Sources Conference, Cherry Hill, New Jersey, 1998, pp. 215–218.
[5] S. Fujiwara, F. Kato, S. Watanabe, M. Inaba, A. Tasaka, Journal of Power Sources 194 (2) (2009) 1180–1183.
[6] L. Redey, R.A. Guidotti, The 37th Power Sources Conference, Fort Monmouth, New Jersey, 1996, pp. 255–258.
[7] R.A. Guidotti, G.L. Scharrer, F.W. Reinhardt, The 39th Power Sources Conference, Fort Monmouth, New Jersey, 2000, pp. 547–551.
[8] P. Masset, Journal of Power Sources 160 (1) (2006) 688–697.
[9] P. Masset, A. Henry, J.Y. Poinso, J.C. Poignet, Journal of Power Sources 160 (1) (2006) 752–757.
[10] P. Masset, J.-Y. Poinso, J.-C. Poignet, The 41st Power Sources Conference, Philadelphia, PA, 2004, pp. 137–140.
[11] P. Masset, S. Schoeffert, J.Y. Poinso, J.C. Poignet, Journal of the Electrochemical Society 152 (2) (2005) A405–A410.
[12] S. Fujiwara, The 43rd Power Sources Conference, Philadelphia, PA, 2008, pp. 121–124.
[13] A. Yuzuru Sato, T. Kojima, Ejima, Journal of the Japan Institute of Metals 41 (12) (1977) 1249–1256.
[14] G.J. Janz, R.P.T. Tomkins, C.B. Allen, J.R. Downey Jr., G.L. Gardner, U. Krebs, S.K. Singer, Journal of Physical and Chemical Reference Data (JPCRD) (1975) 871–1178.
[15] L. Kaufman, H. Bernstein, Computer Calculation of Phase Diagrams with Special Reference to Refractory Metals, Academic Press, New York, 1970, pp. 1–334.
[16] G.J. Janz, F.W. Dampier, G.R. Lakshminarayanan, P.K. Lorenz, R.P.T. Tomkins, Molten Salts: Volume 1, Electrical Conductance, Density, and Viscosity Data, National Standard Reference Data Series (NSRDS), vol. 15, National Bureau of Standards (NBS), 1968, pp. 114–119.